

Article

Transmission Characteristics of Ultrasonic Longitudinal Wave Signals in Negative Refractive Index Materials

Yixue Geng ¹, Yunqiang Sun ^{1,*}, Peng Yang ¹, Xin Liu ² and Jianning Han ^{1,*}

¹ School of Information and Communication Engineering, North University of China, Taiyuan 030051, China; gxt517@outlook.com (Y.G.); s1705069@st.nuc.edu.cn (P.Y.)

² School of Data Science and Technology, North University of China, Taiyuan 030051, China; liuxincn34@hotmail.com

* Correspondence: syq@nuc.edu.cn (Y.S.); hanjn46@nuc.edu.cn (J.H.)

Received: 29 January 2020; Accepted: 19 March 2020; Published: 21 March 2020



Abstract: Longitudinal waves have important applications in modern scientific research and production; as a special acoustic wave, longitudinal waves have a sound transmission performance in negative refractive index materials. This paper has designed a new structure for negative refractive index materials by virtue of COMSOL software and conducted related simulation analysis. Experimental results illustrated that the structure designed had good acoustic longitudinal wave transmission performance. Besides, the effect of sound wave focusing could be achieved by a combination of existing test methods. The design proposed could break the limitation of previous structures on acoustic longitudinal wave transmission. This study is expected to have important implications for the development of solid metamaterial structures.

Keywords: metamaterial; complex structure; ultrasonic wave; longitudinal wave sound field

1. Researches in Ultrasonic Longitudinal Wave Energy Field

Ultrasonic longitudinal wave, also known as P wave, has a wide range of applications in workpiece thickness measurement, defect detection and imaging. As P wave is used for effective detection and accurate quantitative evaluation of defects, the measured area has to be within the longitudinal wave main sound beam to obtain an echo signal with a large amplitude. Therefore, a better understanding of energy distribution law of ultrasonic longitudinal wave sound field has important significance in engineering applications [1].

Many researchers focused their attention on transverse wave and surface wave [2,3]. Jian Ma, for example, analyzed and measured the body wave sound field of an elliptical spot under the oblique incident state of the pulsed laser [4]. However, there is much room to be studied in longitudinal wave sound field.

It was reported that the amplitude variation of ultrasonic longitudinal wave has to be analyzed before acquiring various information of the measurement results in application [5–7]. The energy field distribution of ultrasonic longitudinal waves sound field bears a close relationship with the medium through which the longitudinal waves are transmitted. It seems that much energy has been lost when the waves propagate in a solid medium, and more energy has been lost as the sound is transmitted in high frequency acoustic wave. It was reported that the absorption attenuation is proportional to the square of the frequency of the sound wave and the square of the frequency [8]. Low energy intensity of the energy field caused by severe attenuation of acoustic energy limits the range of application of ultrasonic longitudinal waves. This paper intends to propose a new method for promoting the research of ultrasonic longitudinal wave energy field with the emergence of negative refractive.

2. Negative Refractive Index Material Structure and Acoustic Metamaterial

2.1. The Development of Acoustic Metamaterial Structure

The use of acoustic metamaterials enables the design and manufacture of negative refractive index materials. Negative refractive index material structure was first put forward in 1968, and Ding Changlin et al. noted that Veselago first defined the concept of left-handed materials [9]; the concept of acoustic metamaterials was proposed thereafter. Zhang H F et al. noted that Sigalas et al. [10] proved the existence of the phonon band gap in 1992. Liu et al. clarified the concept of acoustic metamaterials in 2000, marking the beginning of a new phase in the study of acoustic metamaterials [11].

How to realize the negative equivalent parameter is one of the emphases of acoustic metamaterial research [12–16]. In 2005, Professor Liu Zhengyou's team [17] explored the equivalent parameters of three component local resonance structures under long wave conditions and found negative equivalent mass density. In 2006, Professor Mei Jun et al. [18] studied and elaborated a kind of acoustic system composed of cylindrical scatterers embedded in air or water and other fluid media in detail through multiple scattering mechanisms and analyzed its equivalent parameters, pointing out that the negative mass effect is caused by the negative dynamic response of the resonance element. In addition, Li et al. [19] designed a fluid-solid coupling acoustic system by immersing soft silicone rubber in water in 2004 and realized the “double negative” parameters (negative elastic modulus and negative mass density) characteristics. In 2007, Ding et al. [20] designed an artificial periodic structure with double resonators, which combines monopole and dipole resonance and also realized the acoustic “double negative” parameter system. The realization of these “negative refractive index” acoustic parameters indicates that people have been able to see the inherent physical nature of some abnormal acoustic phenomena from the surface, and according to these theoretical basis, we can reverse design and customize the required acoustic super structure materials.

Although acoustic metamaterials found sound application in scientific research at that time, such application was somehow limited due to inadequate theoretical research on the acoustic metamaterials. At present, theoretical research of acoustic metamaterials focuses generally on one dimensional structure; many researchers conduct research based on the spring structure model as Figure 1 shows [21–23]:

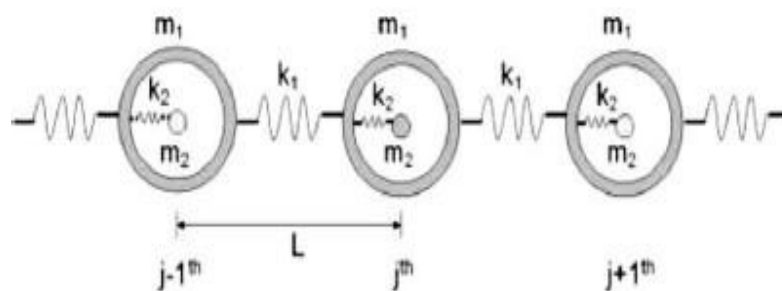


Figure 1. Acoustic metamaterial spring model structure.

Metamaterial structure enables longitudinal waves to transmit effectively and helps enhance the application of sound waves.

2.2. Waveguide Theory of the Acoustic Metamaterial

Considering the basic elastic properties of the isotropic infinite elastic solid, the motion of the medium particle in the solid could be described by the following Equation in the X, Y, Z Cartesian coordinate system [24]:

$$\begin{aligned}\rho \frac{\partial^2 U_x}{\partial t^2} &= (\lambda + \mu) \frac{\partial \Delta}{\partial X} + \mu \nabla^2 U_x \\ \rho \frac{\partial^2 U_y}{\partial t^2} &= (\lambda + \mu) \frac{\partial \Delta}{\partial Y} + \mu \nabla^2 U_y \\ \rho \frac{\partial^2 U_z}{\partial t^2} &= (\lambda + \mu) \frac{\partial \Delta}{\partial Z} + \mu \nabla^2 U_z\end{aligned}\quad (1)$$

In the middle,

$$\Delta = \frac{\partial U}{\partial X} + \frac{\partial U}{\partial Y} + \frac{\partial U}{\partial Z}$$

$$\nabla^2 = \frac{\partial^2}{\partial X^2} + \frac{\partial^2}{\partial Y^2} + \frac{\partial^2}{\partial Z^2}$$

U_x, U_y, U_z represent the displacement vectors of a mass point in the solid in the X, Y, and Z direction, respectively, λ and μ are the pull densities (μ is called the shear elastic coefficient), which also are the density of the solid medium.

By introducing a scalar potential function and a vector potential function, Equation (1) can be expressed as the following two independent equations:

$$\rho \frac{\partial^2 \phi}{\partial t^2} = (\lambda + 2\mu) \nabla^2 \phi \quad (2)$$

$$\rho \frac{\partial^2 \psi}{\partial t^2} = \mu \nabla^2 \psi \quad (3)$$

The potential function can be represented by its component:

$$\rho \frac{\partial^2 \psi}{\partial t^2} = \mu \nabla^2 \psi_i \quad (i = X, Y, Z) \quad (4)$$

The velocity of the medium's particle in all directions can be determined from the potential function:

$$V_x = \frac{\partial U_x}{\partial t} = \frac{\partial \phi}{\partial X} + \frac{\partial \psi_z}{\partial Y} - \frac{\partial \psi_y}{\partial Z} \quad (5a)$$

$$V_y = \frac{\partial U_y}{\partial t} = \frac{\partial \phi}{\partial Y} + \frac{\partial \psi_x}{\partial Z} - \frac{\partial \psi_z}{\partial X} \quad (5b)$$

$$V_z = \frac{\partial U_z}{\partial t} = \frac{\partial \phi}{\partial Z} + \frac{\partial \psi_y}{\partial X} - \frac{\partial \psi_x}{\partial Y} \quad (5c)$$

From Equation (2), in the medium $\psi = 0$, the transmission direction of the wave is X, and $\phi = \phi_A e^{j(\omega t - K_L X)}$, the medium particle velocity can be obtained from (5):

$$V_x = -jK\phi_A \cdot e^{j(\omega t - K_L X)}$$

$$V_y = V_z = 0 \quad (6)$$

Equation (6) describes the law of longitudinal waves, in the medium $K_L = \frac{\omega}{C_L}$; C_L denotes longitudinal wave propagation velocity; $C_L = \sqrt{\frac{\lambda + 2\mu}{\rho}}$ is a constant; ω is the angular frequency of sound waves.

Equation (3) shows the wave propagation direction is still X, and $\phi = 0, \psi_x = \psi_y = 0$. It can be obtained from Equation (5):

$$V_x = V_z = 0$$

$$V_y = jK_t \psi_A e^{j(\omega t - K_t X)} \quad (7)$$

Equation (7) describes the law of the transverse waves and indicates that the particle velocity (Y direction) of the medium is perpendicular to the wave propagation direction X. In the medium, $K_t = \frac{\omega}{C_t}$, C_t denotes transverse wave propagation velocity, $C_t = \sqrt{\frac{\mu}{\rho}}$, ψ_A is a constant.

The theoretical derivation results suggest that transverse and longitudinal waves either coexist or exist alone in solid metamaterials. Waveguide theory of acoustic metamaterials indicates that the propagation velocity of the waves depends only on the nature of the medium when the medium size is infinitely larger than the sound wavelength.

Clearly, designing a new acoustic wave transmission model based on the solid metamaterial structure could help study the transmission and energy field of ultrasonic longitudinal waves effectively.

3. Design of Acoustic Metamaterial Model

Giving priority to the transmission characteristics of high frequency acoustic longitudinal waves, this research firstly analyzed how material equivalent quality varies when resonance frequency changes. Variation curve is illustrated in Figure 2:

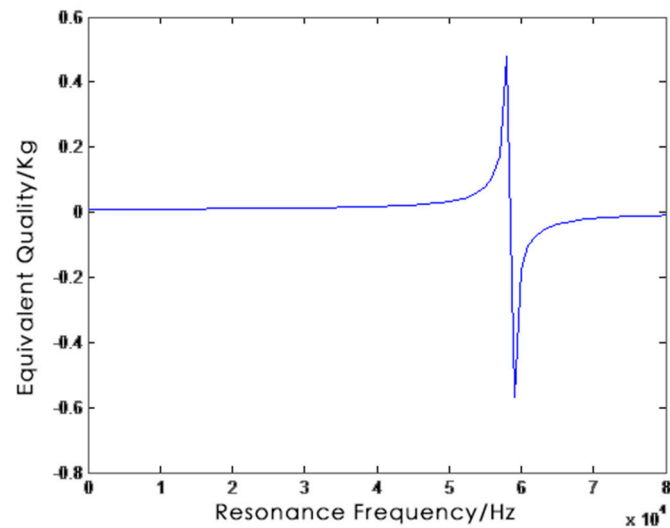


Figure 2. The variation curve of equivalent quality with the changes of resonant frequency.

An acoustical metamaterial design scheme of epoxy rubber lead three-layer structure was adopted and realized by COMSOL software in this paper, as Figure 3 shows:

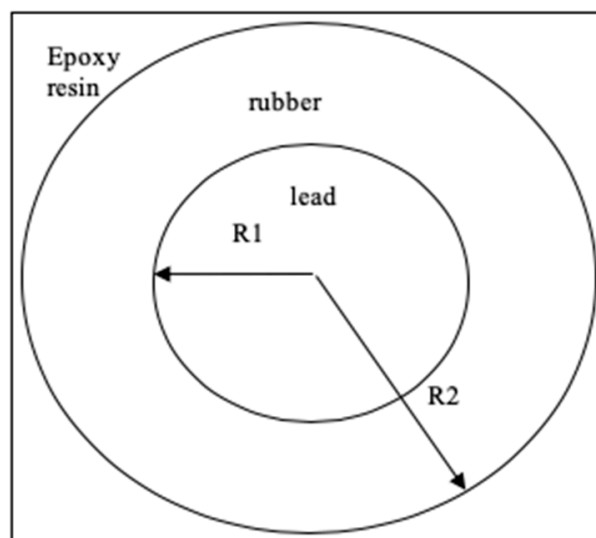


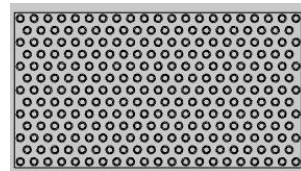
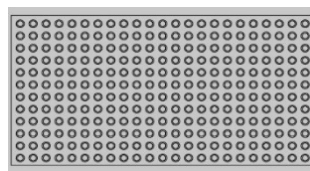
Figure 3. Schematic diagram of the basic structure of acoustic metamaterials.

Figure 3 demonstrates the basic structure of acoustic metamaterials. In the structure designed, the innermost layer was lead, the middle layer was rubber, and the outermost layer epoxy resin. The radius of the lead layer R1 was 1.3 mm, and the thickness of rubber and epoxy was 0.6 mm and 0.3 mm, respectively. The working environment of the model is a water environment, and the outer boundary is set to a perfectly matched layer. Table 1 lists the specifications of the structure designed.

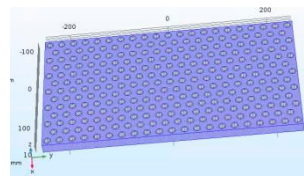
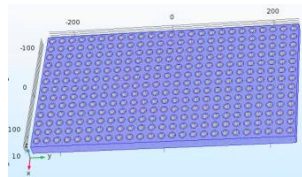
Table 1. Material parameters.

Material	Density ρ ($\text{kg}\cdot\text{m}^{-3}$)	Velocity c ($\text{m}\cdot\text{s}^{-1}$)	Young Modulus E (10^{10} Pa)	Shear Modulus μ (10^{10} Pa)
water	1000	1500	2.19×10^{-1}	
lead core	11600	2160	4.08	1.49
epoxy resin	1180	2680	0.435	0.159
rubber	1300	300	1.175×10^{-5}	4e-6

Based on the basic structure above, an experimental model of solid acoustic metamaterials was projected. Figure 4 illustrates the two-dimensional structure of different specifications of the model.



(a) Rectangular dot matrix arrangement (b) Triangular dot matrix arrangement.



(c) Rectangular dot matrix arrangement. (d) Triangular dot matrix arrangement

Figure 4. The experimental model of solid metamaterials: (a) rectangular dot matrix arrangement; (b) triangular dot matrix arrangement; (c) 3D-rectangular dot matrix arrangement. (d) 3D-triangular dot matrix arrangement.

The one in Figure 4a is of rectangular lattice arrangement, the other in Figure 4b is of triangular lattice arrangement. Figure 4c,d is the three-dimensional structure.

Figure 4c,d reveals that the experimental model is formed by orderly arranging the basic structures on a rectangle substrate with a length $X = 400$ mm and a width $Y = 200$ mm. The model lies the ground for future simulation and test experiments.

4. Simulation Analysis of Model

4.1. Simulation Analysis of Model Effect

Different array schemes were tested to verify the performance of ultrasonic longitudinal wave transmission of the model. The model (Figure 5a) shows was first simulated on COMSOL software, in which the ultrasonic longitudinal wave frequency was 80 kHz. The experiment result is shown in Figure 5b.

Figure 5a illustrates the ultrasonic longitudinal wave propagation direction from the left port (red dot) to the right port (green dot). Figure 5b is a sound field sound pressure distribution diagram after the transmission is stabilized. The red and blue colors indicate the sound pressure values in

different directions, respectively. The deeper the color is, the higher the sound pressure related to the color will be.

Analysis of the simulation effect of Figure 5b shows that, in the sound field, the sound pressure values of the input waves and output waves are primarily the same, indicating that rectangular lattice array model can effectively overcome the energy loss in transmission process; thus, the structure designed has a good ultrasonic longitudinal wave transmission effect.

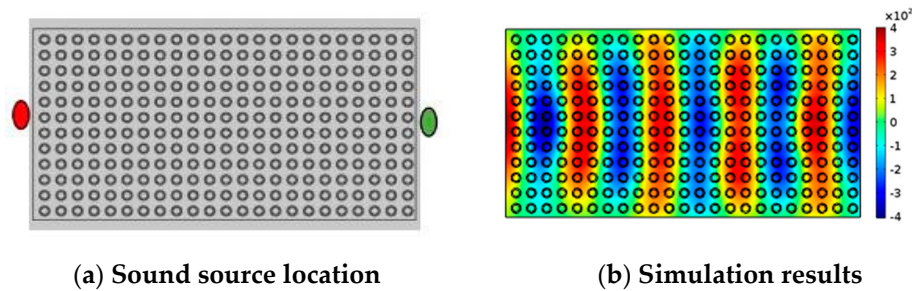


Figure 5. Simulation effect diagram of rectangular dot matrix arrangement scheme: (a) sound source location; (b) simulation results.

Simulation analysis was conducted on the model of triangular lattice arrangement with the conditions unchanged.

The transmission directions of the ultrasonic longitudinal wave in Figures 5a and 6a are identical. Similar to Figure 5b, the sound pressure values of the input almost equal to those of output in Figure 6b. But the sound pressure distributions in sound field in the two pictures are quite different. In Figure 6b, the sound pressure is substantially distributed in linear shape with spaced apart inside the model; in Figure 5b, the sound pressure is of a circle and is distributed mainly at the edge of the model.

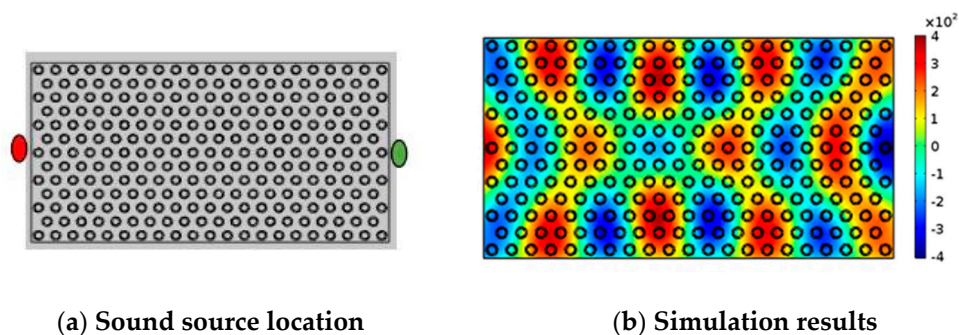


Figure 6. Simulation effect of triangular dot matrix arrangement scheme: (a) sound source location; (b) simulation results.

The sound wave transmission effect in triangular lattice arrangement model is similar to the effect in rectangular lattice arrangement model, but the acoustic wave propagation characteristics of these two models are difference, resulting in diverse sound pressure distributions. This unique phenomenon enables researcher to regulate the transmission of ultrasonic longitudinal waves.

4.2. Transmission Characteristics of Ultrasonic Longitudinal Waves in the Model

The experiments above make clear that the experimental models suggested have good ultrasonic longitudinal wave transmission effect, so further study on the transmission characteristics of ultrasonic longitudinal wave in the models was unfolded on the basis of it. We started our test with the rectangular lattice array scheme, the experimental conditions were same as before, and the experimental phenomenon inside the model was recorded.

Figure 7 is the sound field sound pressure distribution inside the model over different time durations. Figure 7 shows that the ultrasonic longitudinal wave will be linearly transmitted from one side to the other after entering the rectangular arrangement designed model, and a sound pressure distribution in Figure 5b likewise forms when the transmission process is completed. In Figure 7, the color fades during the transmission process, indicating that the sound pressure value tends to decrease in this process. In summary, the model could not completely overcome the problem of acoustic energy loss in wave transmission, but it did have a stable ultrasonic longitudinal wave transmission effect. Besides, there was a significant acoustic energy focusing effect inside the model when the ultrasonic longitudinal wave transmission was stabilized. Moreover, the sound pressure field appeared in the shape of diamond with higher sound pressure value in central portion. This distinct effect can improve the energy density of the ultrasonic longitudinal wave energy field, which has reference meaning to related research.

Then, we manipulated the same test on the model of triangular lattice array. The effect is displayed in Figure 8.

The phenomenon in Figure 8 is highly similar to that in Figure 7. Figure 8 shows the approximately linear sound pressure distribution inside the model during the transmission. The test validated that the farther the sound pressure was from the input point, the lower the sound pressure value would be. The sound field also exhibited an obvious sound energy focusing effect when the transmission was steady.

Differing from the rectangular dot matrix arrangement model, results showed the triangular arranged model had a more pronounced sound energy focusing effect. Moreover, a phenomenon of “polarization” where the sound pressure value at two ends of the sound pressure field was higher emerged, which coincided with the effect in Figure 6b.

Figure 9 is the waveform diagram of the internal sound pressure field distribution of the two models.

Figure 9a is a waveform diagram, showing the sound pressure field distribution inside the model of triangular lattice array. The ordinate is the value of total sound pressure field, and the abscissa is the frequency of ultrasonic longitudinal wave. The green curve is the sound pressure waveform of the ultrasonic longitudinal wave without the model, and the blue curve is the waveform when using the model.

Comparing the two waveforms in Figure 9a, before using the model, the peak value of the ultrasonic longitudinal wave is relatively low, and a large amount of interference signal exists. But when the model is utilized, the sound pressure value in the non-characteristic frequency band is very gentle when the sound pressure value in the characteristic frequency band is significantly higher than that under normal conditions. In a word, the model has clear acoustic focusing effect.

In Figure 9a, the peak on the right side of the blue waveform is higher than the intermediate peaks, indicating that the sound pressure field distribution in the triangular lattice array model has obvious high pressure on two sides. This conforms to the effect as Figures 6b and 8 show.

Figure 9b is the acoustic focusing effect in the rectangular lattice array model, which is similar to the result in triangular lattice array model. However, the difference in Figure 9a,b is that the highest peak of the sound pressure field in characteristic frequency band appears in the middle portion. Moreover, this outcome conforms to the effect in Figures 5b and 7.

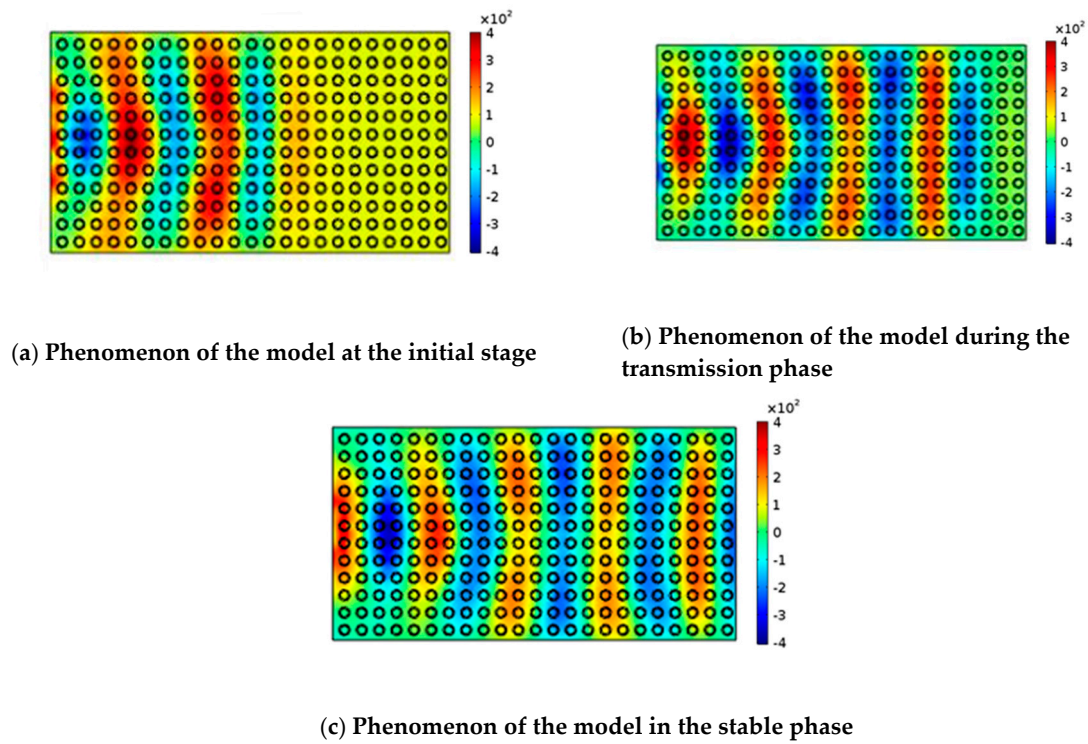


Figure 7. Ultrasonic longitudinal wave transmission phenomenon diagram (rectangular lattice): (a) phenomenon of the model at the initial stage; (b) phenomenon of the model during the transmission phase; (c) phenomenon of the model in the stable phase.

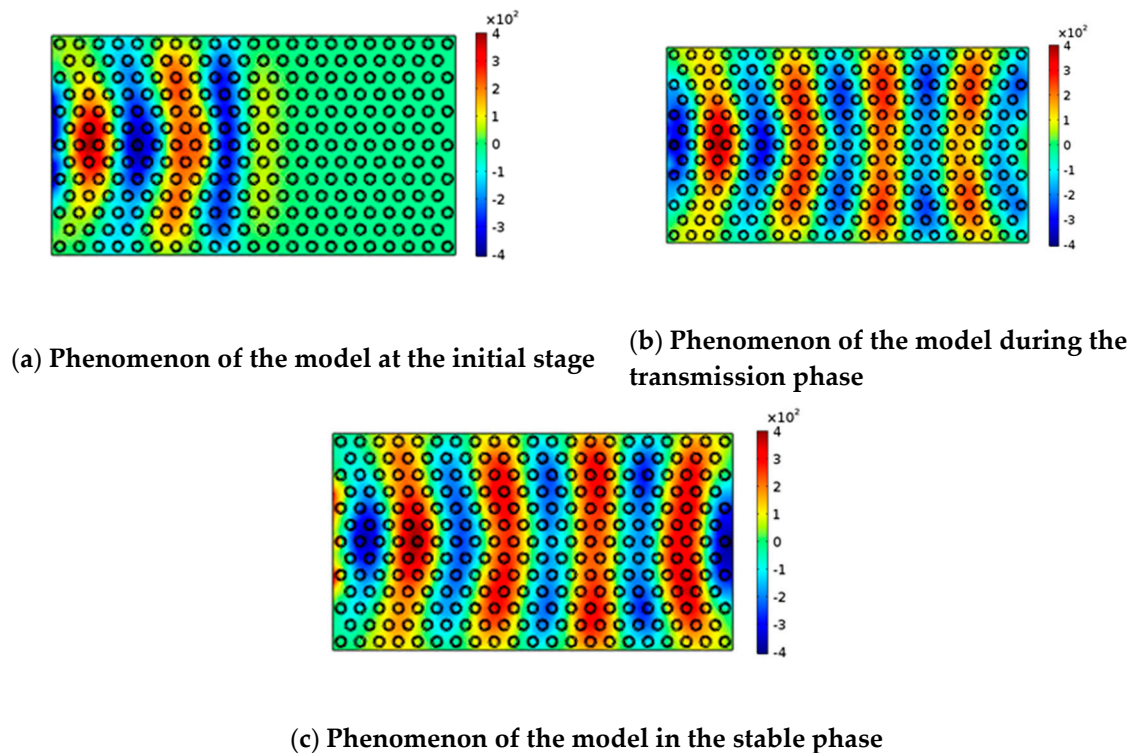
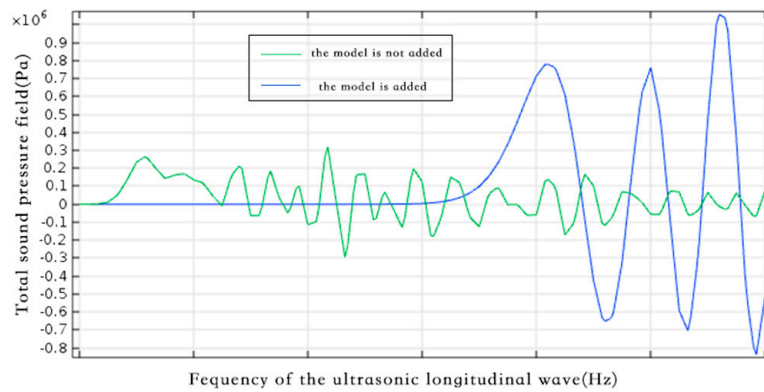
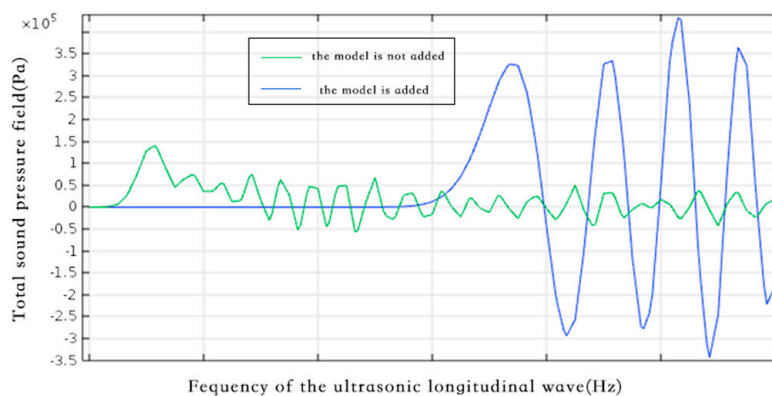


Figure 8. Ultrasonic longitudinal wave transmission phenomenon diagram (triangular lattice): (a) phenomenon of the model at the initial stage; (b) phenomenon of the model during the transmission phase; (c) phenomenon of the model in the stable phase.



(a) Internal sound pressure field (Triangular array)

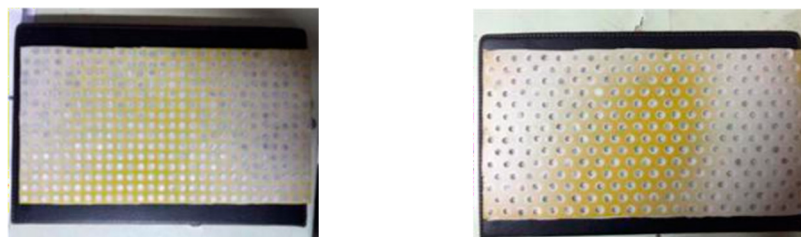


(b) Internal sound pressure field (matrix)

Figure 9. waveform of the internal sound pressure field distribution of the model: (a) internal sound pressure field (triangular array); (b) internal sound pressure field (matrix).

5. Actual Test of the Experimental Model

Figure 10 is the real model with the corresponding specifications produced based on the two experiments conducted above.



(a) Model physical map (Triangular array) (b) Model physical map (matrix)

Figure 10. Schematic diagram of two experimental models: (a) model physical map (triangular array); (b) model physical map (matrix).

Figure 10a is the physical object of the rectangular lattice array experimental model. Figure 10b is the physical object of the triangular lattice array experimental model. Figure 11 illustrates the corresponding test system structure adopted in the next step of the present research.

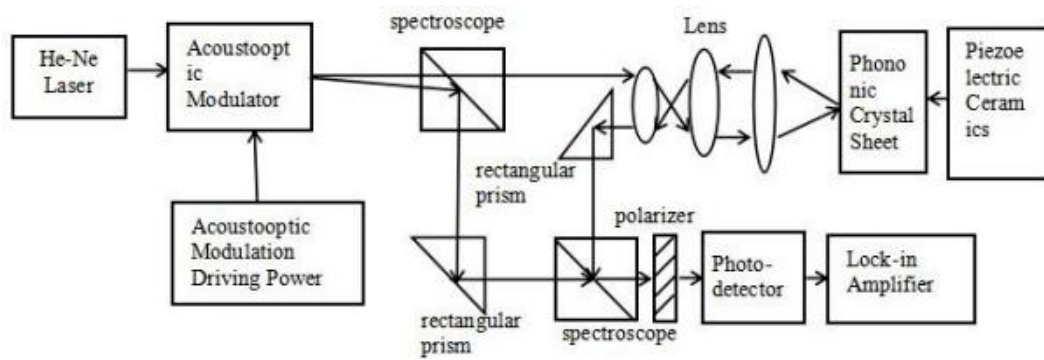


Figure 11. Schematic diagram of the experimental model test system.

Piezoelectric ceramic was used as a receiver to observe sound pressure values, which can convert the received ultrasonic longitudinal wave signal into an electrical signal and then represent the electrical signal. Figures 12 and 13 show the actual experimental environment and the results of the test.



Figure 12. Experimental model actual test system.



(a) Test results (the rectangular dot matrix arrangement model)

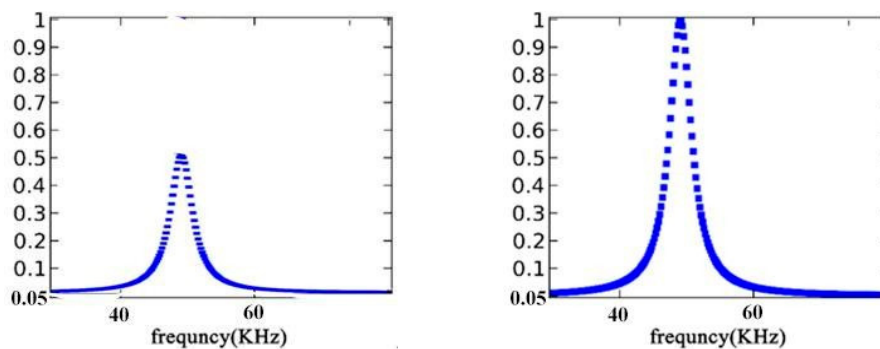


(b) Test results (the triangular dot matrix arrangement model)

Figure 13. Experimental model actual test data record: (a) test results (the rectangular dot matrix arrangement model); (b) test results (the triangular dot matrix arrangement model).

In Figure 13, the left window of the equipment displays the amplitude of the output signal; the middle window represents the phase of the signal, and the right window is the amplitude of the input signal. Figure 13a,b shows the test results of the rectangular dot matrix arrangement model and triangular dot matrix arrangement model, respectively.

Taking the data in Figure 13 and the practical experimental condition of the test platform into account, we sorted out appropriate data to plot the variation curves of frequency response, as shown in Figure 14. It indicates that the amplitude of the same phase signal is extremely enhanced by means of the model, namely, the sound energy is greatly focused. Moreover, comparing with the triangular lattice arrangement, it is close to 1, which is the signal intensity ratio of the rectangular lattice model. This proves that the acoustic energy focusing effect of the rectangular lattice model is better than the triangular lattice array model.



(a) Triangular dot matrix arrangement (b) Rectangular dot matrix arrangement

Figure 14. Signal strength in different arrangements: (a) triangular dot matrix arrangement; (b) rectangular dot matrix arrangement.

6. Conclusions

In conclusion, a new acoustic metamaterial basic structure has been proposed, which innovatively introduces waveguide theory of acoustic metamaterial into the analysis of the transmission characteristics of ultrasonic longitudinal wave. Two different models (rectangular lattice arrangement and triangular lattice arrangement), using the basic structure, have been constructed and simulated on COMSOL software. The simulation results were validated by experiments. The test results demonstrate that both of the models possess good ultrasonic longitudinal wave transmission effect and prominent sound energy focusing effect, but their ultrasonic longitudinal wave transmission effects were different. This offers a method for the regulation of ultrasonic longitudinal waves. The present approach has greatly eliminated the impact of energy loss of ultrasonic longitudinal wave transmission on the formation of energy field, improving the practical application of ultrasonic longitudinal wave.

Author Contributions: Writing-original draft, Y.G.; Funding acquisition, Y.S.; Writing-original draft, P.Y.; Formal analysis, X.L.; Funding acquisition, J.H. All authors have read and agree to the published version of the manuscript.

Funding: This work was supported in part by “The National Natural Science Foundation of China, grant number 61671414”, “The Postdoctoral Science Foundation of China, grant number 2017M611198”.

Conflicts of Interest: The authors declare no conflict of interest. The funders had role in the writing of the manuscript and in the decision to publish the results.

References

1. Wang, Y.; Zheng, X.; Ma, S. Investigation on the longitudinal wave sound field of circular ablation spot. *Laser Infrared* **2018**, *48*, 1468–1472.
2. Liu, P.; Ma, S.; Huang, R. Investigation on the directivity pattern of laser-generated shear wave field. *Laser J.* **2015**, *36*, 40–43.

3. Liu, P.; Ma, S.; Huang, R. Research on directivity of Rayleigh surface wave under linear laser ablation. *Laser Infrared* **2016**, *46*, 1049–1053.
4. Ma, J.; Zhao, Y.; Zhang, Z.; Gao, Y.; Sun, J.; Ju, Y. Acoustic field directivity of longitudinal wave generated by oblique laser based on combustion wave. *High Power Laser Part. Beams* **2016**, *28*, 19–23.
5. Fu, Y.; Zhou, X.; Wei, Z. Study on ultrasonic attenuation propagation in silicone elastomer medium. *J. Zhejiang Univ. Technol.* **1998**, *26*, 184–188.
6. Zhang, Z.; Che, J.; Liu, Z.; Yang, Z.; Zhang, J. Requirement for wave-mode to determine stress intensity factor by ultrasonic wave. *J. Air Force Eng. Univ. Nat. Sci. Ed.* **2001**, *2*, 64–66.
7. Chen, J.; Li, W.; Zhang, Y.; Jin, Y. The laboratory exploration of temperature-dependent characteristics of sound speed in solid. *Phys. Exp. Coll.* **2013**, *26*, 18–20.
8. Ma, D. *Talk of Acoustics*; Hunan Education Publishing House: Changsha, China, 1995.
9. Ding, C.; Dong, Y.-B.; Zhao, X.-P. Research progress on acoustic metamaterials and supersurfaces. *Acta Phys. Sin.* **2018**, *67*, 194301-1–194301-14. (In Chinese)
10. Zhang, H.F.; Maslov, K.; Sivaramakrishnan, M.; Stoica, G.; Wang, L.V. Imaging of hemoglobin oxygen saturation variations in single vessels in vivo using photoacoustic microscopy. *Appl. Phys. Lett.* **2007**, *90*, 053901. [[CrossRef](#)]
11. Liu, Z.; Zhang, X.; Mao, Y. Locally Resonant Sonic Materials. *Science* **2000**, *289*, 1734–1736. [[CrossRef](#)]
12. Huang, H.H.; Sun, C.T.; Huang, G.L. On the negative effective mass density in acoustic metamaterials. *Int. J. Eng. Sci.* **2009**, *47*, 610–617. [[CrossRef](#)]
13. Huang, H.H.; Sun, C.T. Theoretical investigation of the behavior of an acoustic metamaterial with extreme Young's modulus. *J. Mech. Phys. Solids* **2011**, *59*, 2070–2081. [[CrossRef](#)]
14. Chen, H.; Zhai, S.; Ding, C.; Liu, S.; Luo, C.; Zhao, X. Meta-atom cluster acoustic metamaterial with broadband negative effective mass density. *J. Appl. Phys.* **2014**, *115*, 054905. [[CrossRef](#)]
15. Seo, Y.M.; Park, J.J.; Lee, S.H.; Park, C.M.; Kim, C.K.; Lee, S.H. Acoustic metamaterial exhibiting four different signcombinations of density and modulus. *J. Appl. Phys.* **2012**, *111*, 509-R. [[CrossRef](#)]
16. Hao, L.M.; Ding, C.L.; Zhao, X.P. Tunable acoustic metamaterial with negative modulus. *Appl. Phys. A* **2012**, *106*, 807–811. [[CrossRef](#)]
17. Liu, Z.; Chan, C.T.; Sheng, P. Analytic model of phononic crystals with local resonances. *Phys. Rev. B* **2005**, *71*, 014103. [[CrossRef](#)]
18. Mei, J.; Wu, Y.; Liu, Z.; Sheng, P. Effective mass density for periodic solid-fluid composites. *J. Acoust. Soc. Am.* **2012**, *131*, 3372. [[CrossRef](#)]
19. Li, J.; Chan, C.T. Double-negative acoustic metamaterial. *Phys. Rev. E* **2004**, *70*, 055602. [[CrossRef](#)]
20. Ding, Y.; Liu, Z.; Qiu, C.; Shi, J. Metamaterial with Simultaneously Negative Bulk Modulus and Mass Density. *Phys. Rev. Lett.* **2007**, *99*, 093904. [[CrossRef](#)]
21. Han, J.; Tang, S. Acoustic propagation characteristics of heteromorphic metamaterials. *AIP Adv.* **2018**, *10*, 105305.
22. Han, J.; Tang, S.; Wang, R.; Wang, W. Acoustic wave transmission channel based on phononic crystal line defect state. *AIP Adv.* **2018**, *6*, 065201. [[CrossRef](#)]
23. Han, J.; Yang, P.; Tang, S. Local acoustic field enhancement of single cell photoacoustic signal detection based on metamaterial structure. *AIP Adv.* **2019**, *9*, 095064. [[CrossRef](#)]
24. Xiao, S.-H. *Design and Implementation of SAW Filter and Its Frequency Stability*; University of Electronic Science and Technology: Chengdu, China, 2002.

